ELSEVIER

Seminars in
NUCLEAR
MEDICINE

# Positron Emission Tomography/Computed Tomography

David W. Townsend, PhD

**Accurate anatomical localization of functional abnormalities obtained with the use of positron emission tomography (PET) is known to be problematic. Although tracers such as $^{18}$F-fluorodeoxyglucose ($^{18}$F-FDG) visualize certain normal anatomical structures, the spatial resolution is generally inadequate for accurate anatomic localization of pathology. Combining PET with a high-resolution anatomical imaging modality such as computed tomography (CT) can resolve the localization issue as long as the images from the two modalities are accurately coregistered. However, software-based registration techniques have difficulty accounting for differences in patient positioning and involuntary movement of internal organs, often necessitating labor-intensive nonlinear mapping that may not converge to a satisfactory result. Acquiring both CT and PET images in the same scanner obviates the need for software registration and routinely provides accurately aligned images of anatomy and function in a single scan. A CT scanner positioned in line with a PET scanner and with a common patient couch and operating console has provided a practical solution to anatomical and functional image registration. Axial translation of the couch between the 2 modalities enables both CT and PET data to be acquired during a single imaging session. In addition, the CT images can be used to generate essentially noiseless attenuation correction factors for the PET emission data. By minimizing patient movement between the CT and PET scans and accounting for the axial separation of the two modalities, accurately registered anatomical and functional images can be obtained. Since the introduction of the first PET/CT prototype more than 6 years ago, numerous patients with cancer have been scanned on commercial PET/CT devices worldwide. The commercial designs feature multidetector spiral CT and high-performance PET components. Experience has demonstrated an increased level of accuracy and confidence in the interpretation of the combined study as compared with studies acquired separately, particularly in distinguishing pathology from normal, physiologic tracer uptake and precisely localizing abnormal foci. Combined PET/CT scanners represent an important evolution in technology that has helped to bring molecular imaging to the forefront in cancer diagnosis, staging and therapy monitoring.**

**Semin Nucl Med 38:152-166** 

Historically, instrumentation for tomographic imaging of function (single-photon emission computed tomography [SPECT], positron emission tomography [PET]) evolved along a path somewhat different from that of anatomical imaging devices (computed tomography [CT] and magnetic resonance imaging [MRI]) and the corresponding clinical studies were performed and interpreted separately in different clinical services, ie, nuclear medicine and radiology, respectively. Despite this segregation, the usefulness of combining anatomical and functional planar images was evident to physicians even in the 1960s, preceding the invention of CT. The alignment of tomographic images is a complex procedure owing to the large number of degrees of freedom and, without some common features, such coregistration, may be problematic. In addition to simple visual alignment or the use of stereotactic frames that are undesirable or inconvenient in a diagnostic setting, sophisticated image fusion software was developed from the late 1980s onwards.[1] For (relatively) rigid objects, such as the brain, software can successfully align images from MR, CT, and PET, whereas in more flexible

Departments of Medicine and Radiology, University of Tennessee Medical Center, Knoxville, TN.

Financial support for the original PET/CT development was provided by NCI Grant CA 65856.

Address reprint requests to David W. Townsend, PhD, Departments of Medicine and Radiology, University of Tennessee Medical Center, 1924 Alcoa Highway, Knoxville, TN 37920-6999. E-mail: dtownsend@mc.utmck.edu

 0001-2998/08/$-see front matter 
doi:10.1053/j.semnuclmed.2008.01.003

environments, such as the rest of the body, accurate alignment is more difficult because of the large number of possible degrees of freedom. Software fusion is also dependent on matching common features that are extracted either from the images or from markers placed on the patient. Functional imaging modalities such as PET and SPECT often lack reliable anatomical correlates and have coarser spatial resolution and greater noise levels than CT or MR.

One way to address the problems of software fusion is by combining devices (emission and transmission) rather than fusing the images post hoc, an approach that has now coined the term hardware fusion. A combined, or multimodality, scanner such as PET/CT can acquire coregistered structure and function in a single study. The data are complementary, allowing CT to accurately localize functional abnormalities and PET to highlight areas of abnormal metabolism. A further advantage of combined instrumentation is that the anatomical images from CT can be used to improve quantitation of functional images through more accurate attenuation, scatter and partial-volume corrections. This is important in achieving accurate and objective assessment of functional parameters such as myocardial perfusion, tumor uptake values and dosimetry for treatment-planning and monitoring response.

Since the commercial introduction of PET/CT in 2001, adoption of the technology has been rapid, particularly in oncology. Advances in CT and PET instrumentation have been incorporated into the very latest PET/CT designs. In this article, we briefly describe some of the early work that led to the commercial exploitation of PET/CT and subsequently to its current designs. The impact of recent advances in CT and PET performance on these designs will be discussed. An algorithm for CT-based attenuation correction (CT-AC) will be described in addition to the challenges that must be addressed by any implementation of the algorithm in practice.

## Historical Concepts

The origins of tomographic imaging in medicine date from the 1960s or even earlier, but fusion of tomographic images was not explored systematically until the late 1980s.[1] Following the earlier superposition of planar images, in the 1990s 2 principal approaches have emerged to image fusion: software and hardware. The software approach attempts to align 2 image sets post hoc after they have been acquired on different scanners at different times. In contrast, the hardware approach combines the instrumentation for 2 imaging modalities and thus acquires both image sets within the same reference frame and thereby ensures as accurate alignment as possible.

## Image Fusion With Software

Although a complete discussion of the topic is beyond the scope of this chapter, it is instructive to briefly review some of the basic principles of software fusion; a thorough review of software fusion methods can be found in Hawkes et al.[2] Fusion of 2 image sets is achieved either by identifying common landmarks or fiducials that can then be aligned or by optimizing a metric based on image intensity values. Whatever the method, the number of possible degrees of freedom between the 2 image volumes defines the complexity of the subsequent transformation. For distributions that do not involve a change in shape or size, rigid-body transformations are adequate. When shears (or a nonisotropic dilation without shear) are involved, an affine transformation comprising a linear transformation and translation is indicated. When there are no constraints on the deformation, a nonlinear transformation (warp) is used. Although methods involving the alignment of extracted features or fiducials have shown some success, at least for the brain, most current methods are intensity-based and images are coregistered by assessing the intrinsic information content. Metrics include intensity ratios[3] and mutual information.[4] Although such techniques have shown great success in aligning images of the brain acquired with CT, PET, SPECT, and MR, they have been less successful for other parts of the body. Earlier clinical assessment in the lung[5] was disappointing, demonstrating a local registration accuracy of 5 to 8 mm, compared with an accuracy of ~2 mm for the brain.[6] A recent review[7] suggests that software fusion can achieve an accuracy of 2 to 3 mm for some studies.

Commercially available software has improved considerably during the past several years both in the accuracy of the registration algorithms and in the sophistication of the user interface and display. As an example, Hermes Medical Solutions (Stockholm, Sweden) offers advanced fusion software for many clinical applications, including correction of misalignment errors for PET/CT scans, registration of PET/CT scans with MR scans, registration of longitudinal PET/CT studies, alignment of PET and MR scans in Alzheimer's disease and other forms of dementia, and registration of SPECT or PET myocardial perfusion studies with CT or MR scans of the heart. However, despite considerable progress, fusion software will probably never compete with the simplicity and convenience of coregistered studies acquired on a combined PET/CT scanner.

## Multimodality Prototypes

The pioneering work of Hasegawa and colleagues in the late 1980s[8,9] set the stage for the hardware solution to image fusion. The aim of this work was to design a device that could perform emission (radionuclide) and transmission (x-ray) tomography with the same detector (high-purity germanium operated in fast counting mode).[9] Although this approach is attractive, the difficulty is to design a detector that does not compromise performance of at least 1 of the 2 modalities. The work was significant, however, in that it highlighted the strengths of a single device that can perform both anatomical (CT) and functional (SPECT) imaging.[10] Of equal significance was the use of the CT images to generate attenuation correction factors for the emission data.[11] However, recognizing the difficulty of building a detector that would operate optimally for both CT and SPECT, Hasegawa turned to a different design that comprised a clinical SPECT gamma camera in tandem with a clinical single-slice CT scanner.[12]

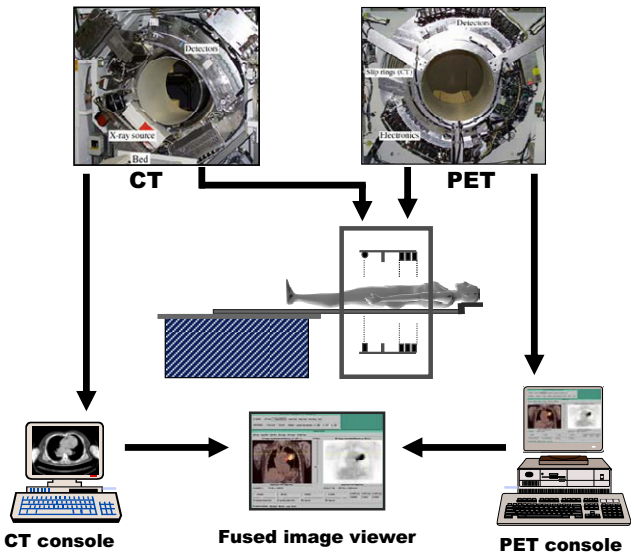


**Figure 1** The first PET/CT prototype evaluated clinically at the University of Pittsburgh. The CT and PET components were mounted on a single rotating support and the data acquired from 2 separate consoles. The CT images were transferred to the PET console and then used for CT-based attenuation correction and localization. (Color version of figure is available online.)

The CT scanner (9800 Quick; GE Healthcare, Milwaukee, WI) was positioned in front of, and aligned with, a scintillation camera (600 XR/T; GE Healthcare). The same bed was used to acquire both studies and the images were registered by taking into account the axial displacement between the CT and SPECT imaging fields of view (FOV). After radiotracer injection and usual uptake period, the patient was imaged first in the CT scanner and then in the SPECT scanner. The CT data were used to generate the SPECT attenuation-correction factors. The combined device was used for a limited number of clinical studies, for example, activity measurements for radiation dosimetry in brain tumor patients.[13]

The proposal to combine PET with CT was made in the early 1990s by Townsend, Nutt and coworkers independently of the Hasegawa work. The suggestion was also made to use the CT images to generate the PET attenuation correction factors.[14] The first prototype PET/CT scanner became operational in 1998,[15] designed and built by CTI PET Systems in Knoxville, TN (now Siemens Molecular Imaging) and clinically evaluated at the University of Pittsburgh. The design incorporated a single-slice spiral CT scanner (Somatom AR.SP; Siemens Medical Solutions, Forchheim, Germany) and a rotating ECAT ART scanner (CTI PET Systems, Knoxville, TN). The PET detectors were mounted on the rear of the CT support and the entire assembly rotated as a single unit (Fig. 1). The data processing included an algorithm[16] to scale the CT images from x-ray energy to PET annihilation photon energy (511 keV) and generate the appropriate attenuation correction factors (as discussed below). Over 300 cancer patients were scanned on the prototype and the findings presented in a series of publications.[17-19] The results from the prototype demonstrated the utility of high-resolution anatomic images accurately registered with functional images. The coregistered anatomy localized functional abnormalities and clarified equivocal situations, thus improving the accuracy and confidence of the scan interpretation. The use of a rapidly-acquired, low-noise CT scan in place of a lengthy conventional PET transmission scan improved image quality and reduced scan time.

## Current PET/CT Instrumentation

In 1999, GE Healthcare launched a dual-head scintillation camera combined with a low-power x-ray tube and detectors, called the Hawkeye (GE Healthcare).[20,21] This design features 2 rectangular sodium iodide camera heads with a 350-W x-ray tube. The Hawkeye was the first commercial scanner to offer combined anatomical and functional imaging in a single unit. Then, less than 2 years after the first Hawkeye installation, PET/CT scanners incorporating clinical CT and clinical PET performance became commercially available. The first commercial PET/CT scanner to be announced was the Discovery LS (GE Healthcare) in early 2001. This was followed several months thereafter by the release of the Biograph (Siemens Medical Solutions), and then somewhat later by the introduction of the Gemini (Philips Medical Systems). In the past 6 years, PET/CT designs from all vendors have evolved following advances in CT and PET instrumentation. By 2007, 5 vendors worldwide offered PET/CT designs: GE Healthcare, Hitachi Medical, Philips Medical Systems, Toshiba Medical Corporation, and Siemens Medical Solutions. Current designs offered by Siemens Molecular Imaging, GE Healthcare, and Philips Medical Systems are summarized in Fig. 2. A recent addition to PET/CT designs is the Gemini TF, the first commercial time-of-flight (TOF) PET scanner.[22] The Gemini TF has yttrium-doped LSO (LYSO) detectors and is combined with a 16- or 64-slice CT scanner. All designs other than the Discovery LS offer a 70-cm-diameter patient port for both CT and PET. All Gemini and Biograph designs acquire PET data in 3D mode only, whereas the Discovery design includes retractable septa and can acquire data in both 2D and 3D mode.

## Advances in Performance for CT and PET

### Multidetector CT Scanners

After the appearance of single-slice spiral CT scanners in the early 1990s,[23] CT performance has experienced a resurgence with the advent of multi-detector arrays (MDCT). This was accompanied by increases in x-ray power (60 kW or greater) and computer capacity for data processing and image reconstruction. Dual- and 4-slice CT scanners first appeared about 1998, with scan times of 500 ms, followed by 16-slice (2002) and, more recently, 64-slice (2004) devices. The increasing number of detector rows (slices) has been accompanied by faster rotation times so that state-of-the-art scanners can now achieve a full rotation in as little as 330 ms. Spatial resolution has improved from ~10 lines pairs (lp)/cm in 1990 to 25

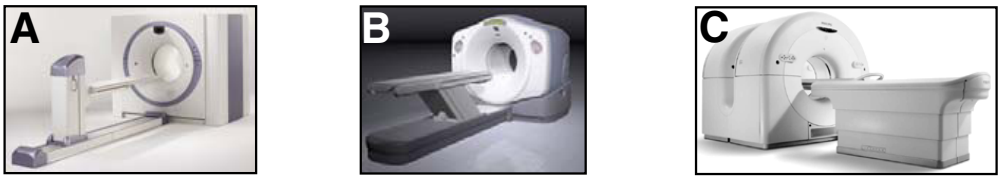


| ***Biograph*** **6, 40, 64** | ***Discovery*** **ST, STE, VCT, RX** | ***Gemini*** ***GXL, TF*** |
|---|---|---|
| **LSO** | **BGO, LYSO** | **GSO, LYSO** |
| 6.4 x 6.4 x 25 $mm^3$ | 4.7 x 6.3 x 30 $mm^3$ (BGO) | 4 x 4 x 30 $mm^3$ (GSO) |
| 4 x 4 x 20 $mm^3$ | 4.2 x 6.2 x 30 $mm^3$ (LYSO) | 4 x 4 x 22 $mm^3$ (LYSO) |
| 3D only (no septa) | 2D/3D (septa) | 3D only (no septa) |
| 6, 40, 64 slice CT | 8, 16, 64 slice CT | 6, 10, 16, 64 CT |
| 70 cm port | 70 cm port | 71.7 cm port |
| 21.6 cm axial FOV | 15.7 cm axial FOV | 18 cm axial FOV |
| 4.5 ns coincidence | 11.7 ns coincidence | 6 ns coincidence |
| bed on rails | dual-position bed | bed support in tunnel |

**Figure 2** Current PET/CT scanner designs from 3 of the major manufacturers of medical imaging equipment: (A) the Siemens Biograph TruePoint, (B) the GE Healthcare Discovery range, and (C) the Philips Gemini series. (Color version of figure is available online.)

lp/cm or better today, with slice thicknesses less than 1 mm. A significant innovation that will contribute to increased CT performance is the low-weight Straton x-ray tube.[24] After many years of slow but steady progress, the past decade has seen significant advances in both hardware and software for CT.

## PET Scanners

This section summarizes recent advances in PET technology that define current PET/CT scanner performance.

### New Scintillators for PET

For PET detectors, the 1970s saw the transition from thallium-activated sodium iodide (NaI(Tl)) to bismuth germanate (BGO), a scintillator with higher density and photofraction. Although at least one PET scanner design continued to use NaI(Tl) until fairly recently, the majority of PET scanners installed during the 1990s were based on BGO block detectors. In the late 1990s, the introduction of new, faster scintillators such as gadolinium oxyorthosilicate (GSO)[25] and lutetium oxyorthosilicate (LSO),[26] both doped with cerium, improved the PET-scanner performance. Both GSO and LSO have shorter decay times than BGO by a factor of 6 to 7, reducing system deadtime and improving count-rate performance, particularly with high activity levels in the FOV. The physical properties of these scintillators are compared in Table 1. Of even more importance for clinical imaging is the potential of faster scintillators to decrease the coincidence timing window, thereby reducing the random coincidence rate. The increased light output of the new scintillators improves the energy resolution because the increased number of light photons reduces the statistical uncertainty in the energy measurement. However, other physical effects contribute to the emission process and the improvement in energy resolution is not a simple function of the number of light photons. The higher light output also increases the positioning accuracy of a block detector, allowing the blocks to be cut into smaller crystals and thereby improving spatial resolution. BGO, LSO, and GSO are not hygroscopic, facilitating the manufacture and packaging of the detectors. GSO is somewhat more fragile and more difficult to machine than either BGO or LSO. LSO has an intrinsic activity concentration (of lutetium-177) of ~280 Bq/mL with single-photon

**Table 1** Physical Properties of PET Scintillators

| Property | NaI | BGO | LSO | GSO |
|---|---|---|---|---|
| Density (g/mL) | 3.67 | 7.13 | 7.4 | 6.7 |
| Effective atomic number | 51 | 74 | 66 | 61 |
| Attenuation length (cm) | 2.88 | 1.05 | 1.16 | 1.43 |
| Decay time (ns) | 230 | 300 | 35 to 45 | 30 to 60 |
| Photons/MeV | 38,000 | 8200 | 28,000 | 10,000 |
| Light yield (% NaI) | 100 | 15 | 75 | 25 |
| Hygroscopic | Yes | No | No | No |

NaI, sodium iodide; BGO, bismuth germinate; LSO, lutetium oxyorthosilicate; GSO, gadolinium oxyorthosilicate.

emissions in the 88- to 400-keV energy range. Such a radioactive component is of little consequence for coincidence counting at 511 keV, except maybe at very low emission count rates.

## Sensitivity

PET is intrinsically a three-dimensional (3D) imaging modality, replacing absorptive physical collimation required for single-photon imaging with the electronic collimation of coincidence detection. The first multi-ring PET scanners incorporated septa, lead or tungsten annular shields mounted between the detector rings. The purpose of the septa was to shield the detectors from photons that scattered out of the transverse plane, restricting the use of electronic collimation to within the plane. Such septa result in inefficient use of the radiation emitted from the patient, but limit scatter and allow 2-dimensional (2D) image reconstruction algorithms to be used. The availability beginning in 1990 of BGO scanners with retractable septa encouraged the use of 3D methodology, at least for the brain, where a 5-fold increase in sensitivity could be realized even with accompanying increases in both scatter fraction and randoms.[27] The situation for whole body imaging is far less favorable, in part because of the presence of significant activity just outside the imaging FOV in most bed positions. Instead, particularly for large patients, 2D imaging has been recommended even though higher administered activities of fluorodeoxyglucose (FDG) are required to obtain adequate count rates. This situation changed in the late 1990s with the introduction of LSO- and GSO-based scanners that could be operated with short coincidence time windows (4.5–6 ns) and higher threshold (400-450 keV) energy windows compared with those of a typical BGO scanner, 10 to 12 ns and 350 keV, respectively. Significantly improved whole-body image quality has been achieved in 3D with a 10 mCi (370 MBq) injection of FDG. Since the LSO and GSO scanners have no septa and acquire data in 3D mode only, no comparison can be made with 2D operation. Within the past several years, a limited number of LYSO (lutetium-yttrium oxyorthosilicate)-based scanners with retractable septa have been evaluated in 2D and 3D and recent publications suggest that 3D is now preferred over 2D operation.[28,29]

The sensitivity of a scanner can also be improved by the addition of more detector material, both in terms of thickness and axial extent. For example, for LSO a 50% increase in thickness (from 20 to 30 mm) results in a 40% increase in intrinsic sensitivity. However, increasing the axial extent by 30% results in a 78% increase in volume sensitivity (for 3D acquisition with no septa). Thus, the latter makes more efficient use of the increased volume of LSO, although there will also be an increase in the number of photomutlipler tubes required (and hence increased cost). Following an injection of a radiotracer such as FDG, the patient potentially receives a radiation dose from all annihilation photons, not just those emitted within the scanner FOV. Therefore, the greater the axial extent (ie, the larger the FOV), the more effective use is made of the emitted radiation and the more efficient use is made of a given volume of scintillator. For most PET/CT scanners, axial PET coverage is ~16 cm, with one design having an axial extent of 18 cm.[22] The most recent design to be announced has an extended FOV covering 21.8 cm axially. The latter comprises more than 32,000, 4 × 4 × 20 mm LSO crystal elements and images 109 2-mm thick transaxial planes per bed position. Data acquisition is fully 3D and the scanner has a peak noise-equivalent count rate (NECR) of ~160 kcps.[30,31]

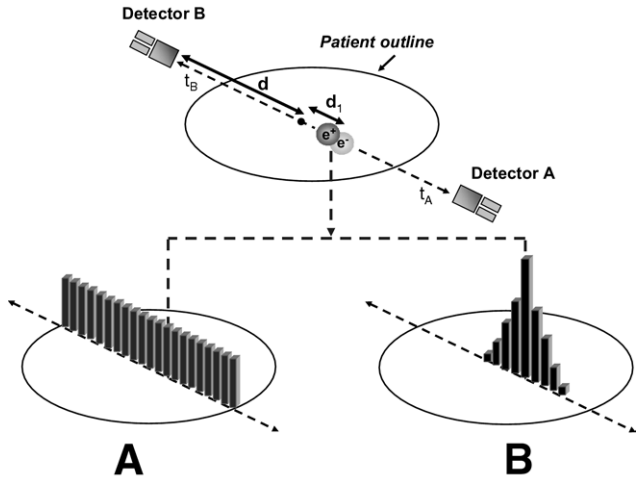


**Figure 3** A schematic diagram illustrating PET data acquisition with the incorporation of TOF reconstruction. By measuring the time difference between the arrival of the 2 annihilation photons, the position of the positron annihilation along the LOR can be localized with an accuracy dependent on the precision of the temporal measurement: (A) without TOF information, the annihilation is located with equal probability along the entire LOR; (B) using TOF information, the annihilation point can be localized to a limited range, eg, a 500-ps timing resolution corresponds to 7.5-cm FWHM spatial range.

## Signal-to-Noise Ratio

The availability of fast scintillators with high stopping power such as LSO and LYSO has revived interest in time-of-flight (TOF) PET,[32] interest that has been further stimulated by the recent announcement of the first commercial PET/CT with TOF, the Philips Gemini TrueFlight (TF).[22] The principle of TOF PET is illustrated schematically in Figure 3. Positron annihilation occurs in the patient at a distance $d+d_1$ from one detector and $d-d_1$ from the other detector. The annihilation photons travel at the speed of light (c), the difference in the arrival times at the detectors between the two photons is therefore $2\ d_1/c$. Photons originating from the center of the FOV ($d_1 = 0$) obviously arrive in the detectors at the same time. Scanners with fast scintillators and electronics can measure this time difference to within a certain resolution. For example, for a scanner with a coincidence timing resolution of 500 ps, the spatial uncertainty on the position of the annihilation is 7.5 cm. This uncertainty is not sufficient to place the annihilation within a 2-mm voxel (and thereby eliminate reconstruction) but it is superior to having no timing information at all and assigning equal probability of the point of emission to all voxels along the line of response (LOR; Fig.

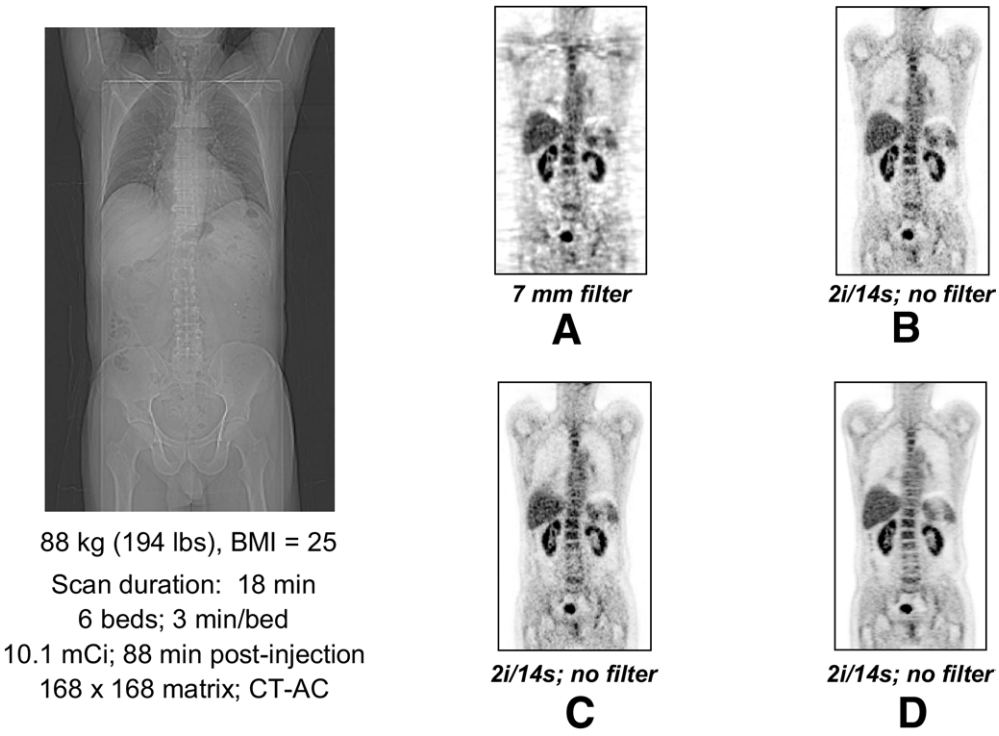


**Figure 4** A coronal section of an FDG-PET whole-body scan of a patient with a body mass index of 25 acquired in 3D mode with septa retracted and reconstructed using: (A) 3D filtered back-projection algorithm with reprojection (7-mm Gaussian smooth); (B) FORE + 2D OSEM (14 subsets, 2 iterations; no smoothing); (C) 3D OP-OSEM (14 subsets, 2 iterations; no smoothing); and (D) HD PET: 3D OSEM with PSF reconstruction (14 subsets, 2 iterations, no smoothing). As noted, all reconstructions except 3DRP are unsmoothed.

3A). Instead, the most probable location of the annihilation is at the center of the uncertainty distribution (Fig. 3B). The TOF information is incorporated directly into the reconstruction algorithm, leading to an improvement in the signal-to-noise ratio (SNR). The increase in SNR is proportional to $\sqrt{(D/\delta d)}$, where D is the diameter of the activity distribution and $\delta d$ is the spatial uncertainty. For a 40-cm diameter uniform distribution of activity and a 7.5-cm uncertainty, the increase in SNR is a factor of ~2.3. As the TOF temporal resolution improves, the spatial uncertainty decreases and the SNR increases by a larger factor. TOF PET was first exploited in the early 1980s[32] with scintillators that were fast but did not have good stopping power for 511-keV photons. Interest declined until the recent emergence of scintillators that are both fast and sensitive. The new TOF PET scanners, based on LSO or LYSO, must demonstrate good timing resolution that is stable over time so as to avoid the need for frequent detector re-calibration. Although promising, the clinical impact of TOF PET has yet to be established. A more detailed review of the published contributions to TOF development can be found in.[33]

## Reconstruction Algorithms

There has been significant progress over recent years in image reconstruction methods through the introduction clinically of statistically based algorithms. Previously, one of the earliest and most widely used 3D reconstruction methods was the re-projection algorithm (3DRP) based on a 3D extension of standard 2D filtered backprojection.[34] Although this algorithm works well for the lower-noise environment of the brain, the quality for whole-body imaging is less than optimal, particularly when rod-source attenuation-correction factors are applied to low-count emission data. Figure 4A, for example, shows a coronal image of a patient with a body mass index of 25 reconstructed using 3DRP. Because CT-based attenuation correction factors have been applied, the image quality is possibly better than would have been obtained with rod-source attenuation-correction factors. The development of Fourier rebinning (FORE)[35] was a breakthrough that enabled 3D data sets to be accurately rebinned into 2D data sets and then reconstructed in 2D with a statistically based expectation-maximization (EM) algorithm. However, it was not until the accelerated convergence achieved by the Ordered-Subset EM (OSEM) algorithm[36] that iterative methods became of clinical interest. Although FORE and OSEM offer improved image quality compared with 3DRP, the incorporation of attenuation-based weights (AWOSEM), as suggested in the original paper by Hudson and Larkin, further improves image quality. This is demonstrated in Figure 4B, where the same data set as in Figure 4A has been reconstructed with FORE and AWOSEM.[37] Further improvement has been achieved by eliminating the rebinning step and implementing OSEM fully in 3D with corrections for randoms, scatter and attenuation incorporated into the system model.[38,39] The result, again for the same data set, is shown in

Figure 4C. Finally, in a recent development termed, "High-Definition (HD)" PET, the detector spatial response function has also been included in the reconstruction model.[40] The point spread function (PSF) varies throughout the FOV owing to the oblique penetration of the detectors by annihilation photons (ie, the depth of-interaction effect). By measuring this variability and then modeling the PSF, improved and near-uniform spatial resolution can be achieved throughout the FOV; the improvement can be seen by comparing Figure 4C with the PSF reconstruction in Figure 4D.

The images in Figure 4 are reconstructed with clinical software provided by a specific vendor (Siemens Molecular Imaging). Of course, most major vendors provide comparable software capable of producing clinical images of high quality. The VUE Point algorithm (GE Health care) is an implementation of 3D OSEM that includes corrections for randoms, scatter, and attenuation and also z-axis smoothing. The Gemini TF (Philips Medical Systems) has TOF capability and therefore the TOF information must be incorporated into the reconstruction.[22] For their Gemini scanner, Philips have implemented a distributed list-mode TOF algorithm that is based on a TOF list-mode Maximum Likelihood approach developed by Popescu and coworkers.[41] They previously used a Row-Action Maximum-Likelihood algorithm (RAMLA).[42] The scatter correction algorithm requires modification to incorporate TOF information. The greatest unresolved effect on image quality, and a challenge to reconstruction algorithms, is now patient size, a significant problem given the current levels of obesity among the US population.

## CT-Based Attenuation-Correction Factors

A recognized strength of PET/CT is the availability of CT images for attenuation correction of the PET data,[16,43] eliminating the need for an additional, lengthy transmission scan. The use of the CT to generate attenuation-correction factors (ACFs) reduces statistical noise. Because the linear attenuation coefficients ($\mu$) are energy-dependent, the CT scan at a mean x-ray energy of ~70 keV must be scaled to the annihilation $\gamma$-ray energy (511 keV). The mean energy of a polychromatic x-ray beam is defined as the energy of a monochromatic beam that would give the same $\mu$ as the polychromatic beam integrated over energy.[44] The polychromatic beam also undergoes beam hardening, the preferential interaction of lower-energy photons as the beam traverses the body causing the mean energy to increase and the corresponding $\mu$ values to decrease.

***Energy scaling algorithm for CT.*** The attenuation of x-rays by tissue depends on the density and the effective atomic number ($Z_{eff}$) of the absorber material. At CT x-ray energies, the physical processes by which photons are attenuated are the photoelectric effect and Compton scattering. The photoelectric probability varies approximately as $Z_{eff}^4$ and scales as $1/E^3$, where E is the photon energy. The Compton scattering probability has little dependence on $Z_{eff}$ and decreases linearly with 1/E. The $\mu$ for a given material is expressed by the sum of the two components:

$$\mu(E) = \rho_e\{\sigma_c(E) + \sigma_{ph}(E, Z_{eff})\}$$

where $\rho_e$ is the electron density and $\sigma_{ph}$ and $\sigma_c$ are the photoelectric and Compton cross sections per electron, respectively. However, at photon energies above about 100 keV in soft tissue, the photoelectric contribution is essentially negligible compared with the Compton-scatter contribution and therefore the expressions for the $\mu$-values at x-ray energy $E_x$ and $\gamma$-ray energy $E_\gamma$ are:

$$\mu(E_x) = \rho_e\{\sigma_c(E_x) + \sigma_{ph}(E_x, Z_{eff})\}$$

$$\mu(E_\gamma) = \rho_e\, \sigma_c(E_\gamma)$$

As a consequence of the 2 separate contributions to $\mu(E_x)$, a single measurement of $\mu(E_x)$ will not uniquely determine $\mu(E_\gamma)$ because, for example, an increase in $Z_{eff}$ could offset a decrease in $\rho_e$ and result in no change in $\mu(E_x)$. In general, therefore, a simple energy scaling of $\mu(E_x)$ is insufficient to yield $\mu(E_\gamma)$. By restricting the problem to biological tissues for which $Z_{eff}$ are all fairly comparable and noting that the contribution from $\sigma_{ph}$ is relatively small even at x-ray energies, changes in $\mu(E_x)$ are primarily caused by changes in tissue electron density. Thus, for the limited range of biological tissues, a single scaling factor can be used to convert $\mu(E_x)$ to $\mu(E_\gamma)$ for lung, liver, fat, muscle, and other soft tissues. For spongiosa and cortical bone, however, the same scale factor will not apply because of the significant calcium and phosphorous content of bone that result in a higher $Z_{eff}$ different from those of soft tissues.

This issue has been addressed[16] by segmenting bone from soft tissue at a specific threshold and applying different scale factors to the two different tissue classifications—bone and nonbone—corresponding to different values of $Z_{eff}$. Kinahan and coworkers adopted a threshold of 300 Hounsfield units (HU).[16] Subsequently, Watson and coworkers[44] proposed a mixture model in which all tissues with $\mu$ less than $\mu$(water) are treated as a mixture of air and water at various concentrations, while tissues with $\mu$ greater than $\mu$(water) are treated as a mixture of water and cortical bone. Since this approach limits the composition to a single value for a given $\mu(E_x)$, a bi-linear scaling function can be defined for biological tissues, as shown in Figure 5. Recent publications on CT-based attenuation correction for PET also propose a "break-point" at 0 HU (corresponding to $\mu$(water)),[45] although a more appropriate choice may be slightly greater than zero, ~60 HU, because some soft tissues and blood conform to the air-water mix but with densities greater than water.

The calibration function has been derived from phantom measurements and has also been validated with patient data.[46] The calibration of the CT scanner ensures that the soft-tissue values ($\mu < 60$ HU) are independent of the kVp setting of the x-ray tube. This independence does not apply to bone-like tissue ($\mu > 60$ HU) and therefore different calibration functions are required for each kVp setting.[47]

The CT scan is acquired before the emission data so the

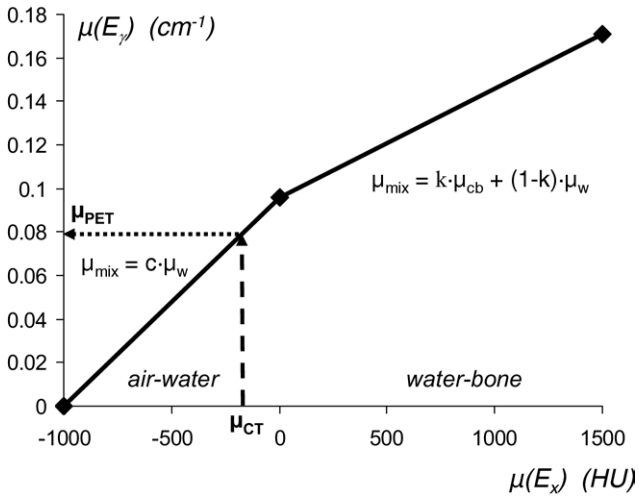


**Figure 5** The bi-linear scaling function used to convert CT numbers (Hounsfield Units, HU) to linear attenuation coefficients ($\mu$) at 511 keV. The attenuation-correction factors are generated by reprojecting the $\mu$-map at 511 keV. w = water and cb = cortical bone; k is the concentration of the components of the mixture.

ACFs can be generated for the entire volume. The CT images are first rebinned to the spatial resolution of the emission data. The images are next scaled voxel-by-voxel to the energy of the emission data by applying the bi-linear scaling function (Fig. 5). The scaled CT images are then forward projected to generate ACFs that match the sampling of the emission data. Since the introduction of the PET/CT scanner, CT-based attenuation correction has been a significant focus of research to address the various possible artifacts. The following sections will review the status of this work and the outstanding challenges that remain for CT-based attenuation correction.

## Artifacts Specific to CT-Based Attenuation Correction

Although the benefits of CT-based attenuation are now well known and documented, a number of challenges have emerged as the technique has become more widely adopted for PET/CT.[48,49] There are 2 main concerns (1): the presence of materials in the patient with $Z_{eff}$ values that do not conform to the basic assumptions in the bilinear model and (2) mismatch between the CT and PET caused by patient respiration, cardiac motion, and bowel movement.[50] Since the first commercial PET/CT installation in 2001, these issues have received considerable attention. Examples of (1) above include metallic objects,[51,52] dental hardware,[53] calcified lymph nodes, and intravenous[54,55] and oral contrast.[56,57] Materials with high $Z_{eff}$ may even exceed the dynamic range of attenuation values measurable by CT and severe image artifacts can result. Of particular importance in the assessment of head and neck cancer is the presence of dental fillings.[53] A number of metal-artifact reduction techniques have been explored,[58] including modified reconstruction methods[59] and segmentation approaches[60] that can significantly reduce the artifacts.

Some characteristic artifacts associated with CT-based attenuation correction are illustrated in Figure 6. When tidal breathing is adopted for both CT and PET, respiration effects

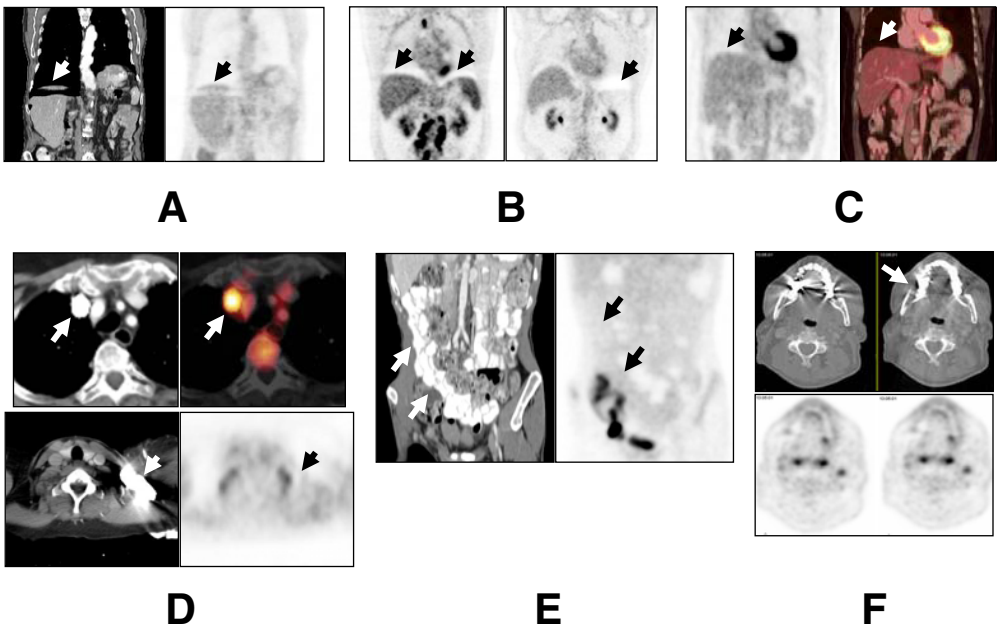


**Figure 6** Potential image artifacts generated from CT-based attenuation correction: (A) an artifact caused by respiration in which the dome of the liver is displaced into the base of the right lung; (B) curved photopenic areas above the liver and spleen caused by CT and PET mismatch from respiratory movement of the diaphragm; (C) an example of a well-registered study that is free of artifacts; (D) the variable effects of intravenous contrast showing an artifact on the PET image (top row) caused by a contrast bolus and the absence of an artifact on PET (bottom row); (E) the effect of oral contrast where the presence of contrast in the GI tract does not cause an artifact on the PET image (arrow); and (F) the effect of dental fillings on the CT and PET images.

include an apparent displacement of the dome of the liver into the lower lobe of the right lung (Fig. 6A),[61] creating a corresponding region of apparent activity on the PET scan (arrow). A curved photopenic region at the top of the liver and spleen in the PET image (Fig. 6B) is also observed in some studies. Although such artifacts may occur for any patient following a tidal breathing protocol,[62] the documented incidence is much lower for faster, higher-performance CT scanners. Figure 6C is an example of a study, acquired on a 6-slice CT scanner, that shows no evidence of breathing artifacts or misregistration. The clinical significance of respiratory artifacts has been studied for an early PET/CT design in a series of 300 patients[63] and was found to result in ~2% incorrect diagnoses.

### Intravenous Contrast

The use of intravenous contrast may be indicated when the CT scan is performed for clinical purposes as opposed to low-dose CT performed for attenuation correction and localization only. Intravenous contrast contains iodine at concentrations high enough to enhance CT values without a corresponding change in density, and it is used in CT to enhance $\mu$ values in the vasculature by increasing the photoelectric absorption compared with the blood. CT contrast results in a 40% change in attenuation at CT x-ray energies whereas at 511 keV where the photoelectric effect is negligible, contrast has only a 2% effect or less.[64] However, if contrast-enhanced tissue voxels are misidentified as a water-bone mix, the scaling factor will be incorrect and the erroneously scaled pixels may generate artifacts in the PET image (Fig. 6D, top row).[65] Tens of thousands of PET/CT scans have now been performed in the presence of intravenous contrast and experience has shown that contrast administration does not generally cause a problem that could potentially interfere with the diagnostic value of such scans.[54,66,67] This is largely due to the fact that intravenous contrast is rapidly dispersed throughout the vascular system. An exception may be the passage of the contrast bolus through a major vessel, although even this does not always generate an artifact on the PET image (Fig. 6D, bottom row). Optimized CT protocols have been developed for the administration of intravenous contrast that avoid most of the foregoing issues.[68] A recent publication[69] has documented a rate of 2 patients per 100 where an incorrect management decision would have been made because of the use of noncontrast, low-dose CT acquired for localization and CT-AC only.

### Oral Contrast

Oral contrast is administered to enhance radiographic visualization of the gastrointestinal tract. Its distribution is somewhat variable, however, both in spatial distribution and level of enhancement. Modifications to the basic scaling algorithm have been introduced to distinguish oral contrast-enhanced voxels from bone pixels.[64] As with intravenous contrast, there is little evidence that the presence of oral contrast results in diagnostic errors of any significance.[70] Figure 6E shows a patient imaged with oral contrast; enhancement of the colon on the CT image (left; arrows) shows no corresponding artifactual uptake on the PET image (right). Nevertheless, in some protocols, contrast CT is performed in addition to the low dose CT for attenuation correction and localization, thereby increasing the radiation dose to the patient. However, a low-dose whole-body CT in addition to a clinical CT with contrast over a limited axial range (single PET bed position) may involve less radiation dose than a whole-body clinical CT with contrast. Of course, CT AC problems with oral contrast can be eliminated entirely if negative contrast agents such as mannitol or even water are used instead of the usual high-Z agents.[71]

### Metal Implants

Dental artifacts can be corrected on CT through the use of novel reconstruction techniques,[59] as shown in Figure 6F. The uncorrected (left) and corrected (right) images for CT (top) and PET (bottom) demonstrate that the reconstruction algorithm significantly improves the CT image without affecting the PET image, verifying that CT-based attenuation correction is actually a robust technique. Although metallic implants such as artificial hip prostheses can sometimes cause artifacts on CT, this appears to be due more to patient movement between the CT and the PET scan than to the presence of prostheses per se.[72] The nonattenuation-corrected image is, in any case, available to resolve ambiguities.

### Respiratory Motion

In recent years, the most widely addressed issue related to CT-based attenuation correction has been respiratory motion[73-76] and the artifacts created by the mismatch between CT and PET.[77] These issues are addressed in detail in the accompanying article by Nehmeh and Erdi in this volume and are only briefly discussed here. Rotating[68] Ge sources used in conventional PET scanners results in a transmission scan that averages patient respiration in a way compatible with the corresponding emission scan. The use of CT-AC suggests a number of different protocols must be explored to resolve the mismatch problem. For example, the advent of fast, spiral CT scanners made breath-hold CT a reality, although clinical images are typically acquired with full inspiration to separate lung structures. Such an expansion of the chest does not match a PET scan acquired with shallow breathing and results in serious attenuation correction artifacts in the anterior chest wall. The appearance of artifacts due to respiratory motion and the spatial and temporal mismatch between CT and PET images has led to intensive research to identify the best respiratory protocol. A number of different protocols have been explored, including:

- Continuous shallow breathing for both CT and PET[73];
- CT scans acquired over the diaphragm with limited breath hold[73];
- Breath-hold CT acquired with partial inspiration[73];
- Motion-averaged CT over many respiration cycles[78,79];
- Cine CT acquiring a full breathing cycle per slice[80];
- Respiratory-gated CT plus shallow-breathing PET[81];
- Deep-inspiration breath hold[82,83];
- Breath-hold CT plus gated PET[84,85];
- Respiratory-gated CT and PET.[86]

Currently, the simplest and most widely used protocol is shallow breathing for both CT and PET.[73] Early single- or

dual-slice PET/CT designs exhibited a high incidence of breathing artifacts (Fig. 6A and B).[62] However, with the incorporation of fast MDCT into PET/CT scanners, the incidence of such artifacts has been greatly reduced. Nonetheless, the CT images still do not exactly match the motion-averaged PET acquisitions and protocols such as slow CT acquisition have also been explored. The clinical significance of these attenuation–correction effects continues to be debated, particularly with respect to lesions in the base of the lung and dome of the liver where curved photopenic areas are observed (Fig. 6B). Displacement of such lesions may result in incorrect localization or, worse, a failure to identify them correctly thus leading to misdiagnosis. Shallow breathing during PET/CT has been shown to be inadequate for the comprehensive staging of lung cancer.[87] Nevertheless, a significant percentage of studies acquired on even a 6-slice CT scanner show good registration with shallow breathing.

Finally, 2 other effects can also influence the accuracy of CT-AC: the truncation of the transverse FOV[88] and the presence of scattered radiation. Truncation of the FOV arises because typically CT scanners have a 50-cm diameter and PET scanners a 60- to 70-cm diameter FOV. Simple software extrapolation techniques have proved effective in extending the CT FOV to match that of PET, at least with an accuracy adequate for CT-AC.[89,90] Scatter is increased by imaging with the patient's arms in the FOV. However, the short scan times achievable with state-of-the-art PET/CT allow almost all patients to tolerate imaging with their arms raised, reducing the effects resulting from increased scatter. (Head-and-neck cancer patients, of course, continue to be scanned with their arms down.)

Despite the artifacts and other issues discussed previously and occasional opinions to the contrary,[91] CT-based attenuation correction has become the de facto standard for PET/CT. The advantages, which include convenience and short acquisition times, largely outweigh the drawbacks. In a small number of studies, quantitative comparisons have been made between ACFs generated from standard PET transmission scans and from CT[75,92,93] and, even though some differences in SUV values have been noted, nothing of diagnostic significance has been documented.

# Radiation Dose Considerations

The radiation exposure to the patient from a PET/CT scan is both external, from the CT scan, and internal, from the injected PET radiotracer,[94] and has emerged as an issue of some concern.

## External Dose

Dose assessment in CT is challenging and depends not only on the body region exposed but also on a variety of scan-specific parameters, including tube potential (kVp), tube current and exposure time (mAs), slice collimation, and pitch.[95] In addition, the dose also depends on certain technical features of the scanner, such as beam filtration, beam-shaping filter, geometry, and acquisition algorithm. Therefore, values for CT patient dose vary considerably among centers and among scanners. For whole-body CT scans that extend from the level of the thyroid to the symphysis, the effective CT dose $E_{ext}$ can be estimated approximately as follows:

$$E_{ext} = \Gamma_{CT} \cdot CTDI_{vol}$$

where $\Gamma_{CT} = 1.47$ mSv/mGy is the dose coefficient that relates the volume CT dose index $CTDI_{vol}$ to the effective dose. For a typical set of clinical scan parameters, the $CTDI_{vol}$ is 13 mGy[96] resulting in a total effective whole-body dose of 19 mSv. However, many centers acquire the CT scan for attenuation correction and localization only, reducing the whole-body dose to as low as 3 mSv or even lower. In addition, there are a number of strategies to make more efficient use of the radiation, such as tube current modulation and automatic exposure control.[97,98]

## Internal Dose

The internal radiation dose will depend on the biodistribution and the physical and biological half-life of the radiotracer as well as the activity administered to the patient. The dose is generally expressed as the effective dose and the absorbed doses to the whole body and to the individual major organs. The effective dose $E_{int}$ resulting from administration of activity A of a given radiotracer can be estimated from the following:

$$E_{int} = \Gamma \cdot A$$

where $\Gamma$ is a dose coefficient computed for the adult hermaphrodite Medical Internal Radionuclide Dosimetry phantom. Currently, the principal radiotracer of interest is FDG, for which the dose coefficient is 19 $\mu$Sv/MBq,[99] although a higher dose coefficient of 29 $\mu$Sv/MBq has also been published.[100] As for phantom-based dosimetry generally, the foregoing FDG dose coefficient applies to patients whose body habitus reasonably approximates that of the 70-kg adult hermaphrodite phantom. It is neither age- nor gender-specific and does not account for differences among individuals in terms of their FDG pharmacokinetics. Dose coefficients for adult females (based on 54-kg anthropomorphic model) and for younger individuals (based on low body-mass models) are now also available.[101] Based on the published value[99] for the dose coefficient, the average whole-body dose for a typical 10-mCi (370-MBq) administered activity of FDG is 7 mSv. However, most radiotracers do not distribute uniformly in the body, and, for example, the critical (ie, highest-dose) organ for FDG is the bladder due to its primarily urinary excretion.

## Total Dose

The total dose for PET/CT is, of course, the sum of the internal and external doses. For a diagnostic CT and FDG PET scan, the effective dose is ~25 mSv. However, this can be reduced to 10 mSv or less if a low-dose CT—for localization and attenuation correction only—is acquired. In practice, the PET/CT dose to a specific organ will depend on the exact protocol; for example, if the CT scan does not include the

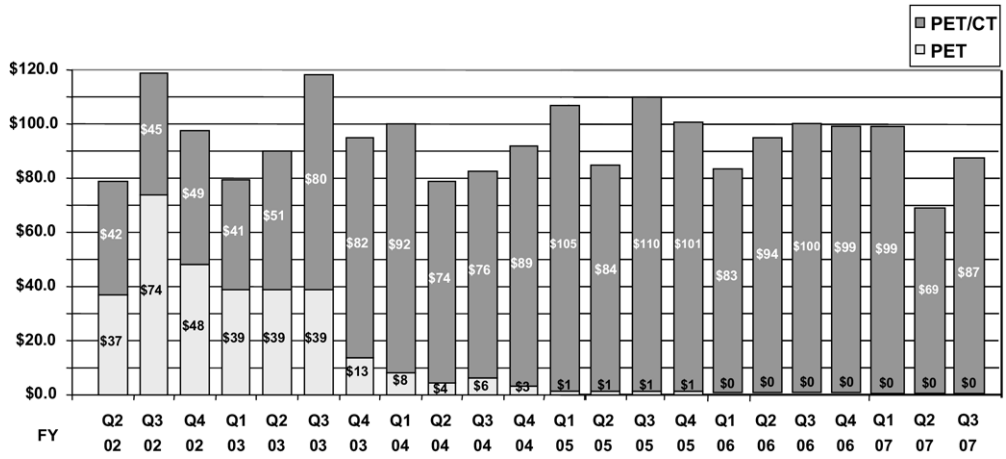


**Figure 7** Shipments of PET and PET/CT scanners for the U.S. market as recorded by the Nuclear Equipment Manufacturers Association for the period January 2002 to October 2007. Note that the figures (in $M) reflect the total revenue for all shipments from which the selling price and individual unit type cannot be determined. Shipments of PET-only scanners declined during this period to zero from January 2006 onwards. The overall market for PET or PET/CT remained fairly constant throughout this period, although since January 2007, with the reduction in reimbursement due to the introduction of the Deficit Reduction Act, sales have declined somewhat.

bladder, the dose to the bladder wall will be due entirely to FDG. For a smaller patient and a higher-sensitivity scanner, a lower FDG dose can be used, potentially limiting the effective dose to 5 mSv or less. In comparison, the world-wide average annual dose due to the natural radioactive background is 2.4 mSv.

## The Clinical Role of PET/CT

Before the introduction of PET/CT, essentially all multimodality clinical imaging was based on software fusion techniques[7] and limited mainly to the brain. The introduction of the Hawkeye (GE Healthcare) in 1999, followed less than 2 years later by the first commercial PET/CT scanner, has irreversibly transformed the field of multimodality imaging. From 2001 to 2006, the sales of PET-only scanners decreased to 0, being replaced entirely by sales of PET/CT (Fig. 7). Currently, in 2008, a worldwide installed base of more than 2000 units attests to the rapid adoption of the modality by physicians.

The majority of this installed base is in routine clinical operation and there is, at least for oncology, a growing body of literature that supports the improved accuracy of staging and re-staging with PET/CT compared with either CT or PET acquired separately.[102,103] Many of the pertinent publications have appeared within the past 2 to 3 years, and clearly document significant improvements in specificity and, to some extent, also in sensitivity, and especially in early detection of cancer recurrence.[104] These improvements are incremental when compared with PET, which alone demonstrates high sensitivity and specificity for a wide range of diseases. Improved accuracy has been documented for a variety of cancers including head and neck,[58,105] thyroid,[106] lung,[107-109] breast,[110,111] esophageal,[112,113] colorectal,[114,115] and melanoma.[116] There is also evidence that PET/CT improves accuracy in lymphoma[117] and solitary pulmonary nodules,[118,119] despite the fact that in lymphoma the accuracy of PET alone is already very high.[120]

In summary, therefore, the improvement in accuracy of PET/CT compared with PET or CT for staging and restaging is statistically significant and averages 10%-15% over all cancers.[103] As an illustration, Figure 8 shows 2 studies acquired on a Biograph 6 TruePoint TrueV PET/CT (Siemens Molecular Imaging) with a 21.8-cm axial FOV. Figure 8A shows transaxial PET and fused images of a 50-year-old woman diagnosed with pancreatic cancer. The images demonstrate intense focal uptake of FDG in a primary neoplasm 3.4 × 2.6 cm in size that can be accurately located in the head of the pancreas. No FDG uptake was identified in any of the proximal nodes although the likelihood of micrometastases would be high. Figure 8B shows a 58-year-old female patient with metastatic renal cell cancer. The images were acquired 110 minutes after the injection of 9.7 mCi of FDG. The total scan duration was 15 minutes with acquisition of 5 bed positions at 3 minutes per position. The CT was acquired at 130 kVp and 180 mAs (Siemens CAREDose). The study demonstrates a large FDG-avid peripherally enhancing necrotic mass occupying the anterior mid- and lower-left kidney. The mass is 10 cm in size and appears to involve the lower-pole collecting system.

## Conclusion

There is little doubt that, during the past 6 years, PET/CT has had a growing impact on clinical imaging and particularly in oncology in staging and restaging disease and monitoring response to therapy. Although the technology has been somewhat disruptive in the sense that it has brought together medical specialties that have not traditionally worked together, namely, nuclear medicine and radiology, the overall

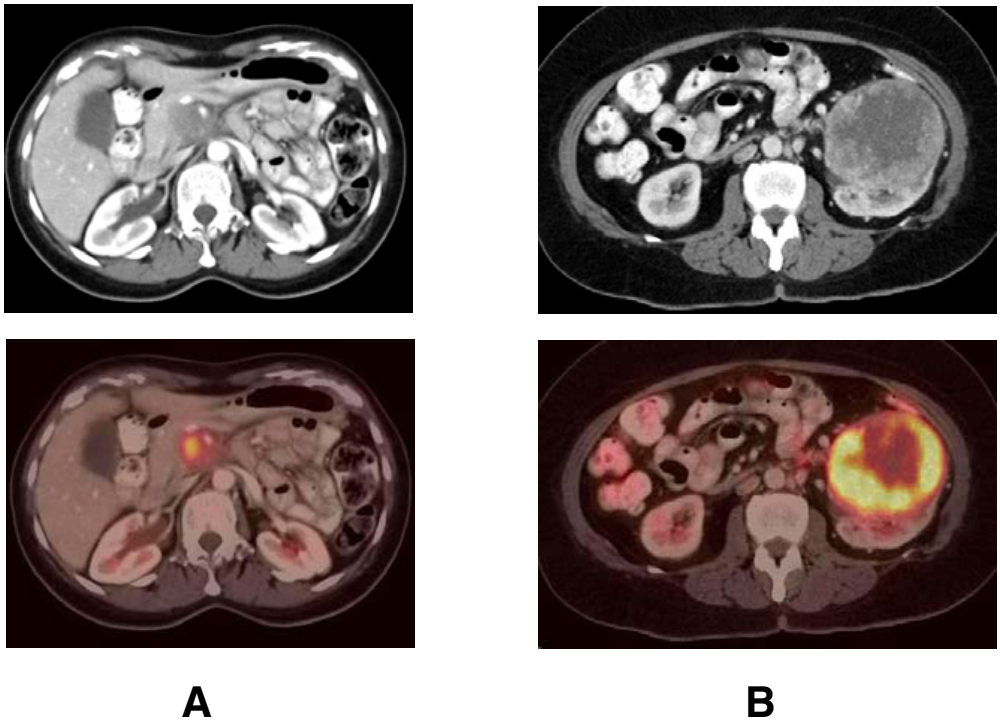


**Figure 8** Two studies acquired on a Biograph 6 TruePoint TrueV PET/CT scanner. Transaxial sections are for PET (top row) and fused images (bottom row). (A) A 50-year-old woman with a diagnosis of pancreatic cancer. The images were acquired 94 minutes after injection of 10.3 mCi of FDG. The total scan duration was 10 minute with acquisition of 5 bed positions at 2 minutes per position. The CT was acquired at 130 kVp and 180 mAs (Siemens CAREDose). (B) A 58 year-old female patient with metastatic renal cell cancer from an unknown primary. The images were acquired 110 minutes after injection of 9.7 mCi of FDG. The total scan duration was 15 minutes with acquisition of 5 bed positions at 3 minutes per position. The CT was acquired at 130 kVp and 180 mAs (Siemens CAREDose).

impact has been positive. To meet the demand for cross-training of both the technologists who operate the devices and the physicians who interpret the studies, guidelines have been published[121] and new standards established, leading to a somewhat different situation today from the way radiology and nuclear medicine have traditionally functioned. This trend is likely to continue as other multimodality devices reach the clinic, including SPECT/CT (introduced in 2004) and MR/PET (currently under development).

## Acknowledgments

Dr. Townsend is a senior consultant with Siemens Molecular Imaging, Knoxville, TN, that manufactures and markets a combined PET/CT scanner.

## References

1. Levin DN, Pelizzari CA, Chen GT, et al: Retrospective geometric correlation of MR, CT, and PET images. Radiology 169:817-823, 1988
2. Hawkes DJ, Hill DL, Hallpike L, et al: Coregistration of structural and functional images, in Valk P, Bailey DL, Townsend DW, et al (eds): Positron Emission Tomography: Basic Science and Clinical Practice. New York, Springer-Verlag, 2003, pp 181-198
3. Woods RP, Mazziotta JC, Cherry SR: MRI-PET registration with automated algorithm. J Comput Assist Tomogr 17:536-546, 1993
4. Maes F, Collignon A, Vandermeulen D, et al: Multimodality image registration by maximization of mutual information. IEEE Trans Med Imaging 16:187-198, 1997
5. Wahl RL, Quint LE, Cieslak RD, et al: "Anatometabolic" tumor imaging: Fusion of FDG PET with CT or MRI to localize foci of increased activity. J Nucl Med 34:1190-1197, 1993
6. West J, Fitzpatrick JM, Wang MY, et al: Comparison and evaluation of retrospective intermodality brain image registration techniques. J Comput Assist Tomogr 21:554-566, 1997
7. Hutton BF, Braun M: Software for image registration: Algorithms, accuracy, efficacy. Semin Nucl Med 33:180-192, 2003
8. Hasegawa BH, Gingold EL, Reilly SM, et al: Description of a simultaneous emission-transmission CT system. Proc SPIE 1231:50-60, 1990
9. Hasegawa BH, Stebler B, Rutt BK, et al: A prototype high-purity germanium detector system with fast photon-counting circuitry for medical imaging. Med Phys 18:900-909, 1991
10. Lang TF, Hasegawa BH, Liew SC, et al: Description of a prototype emission-transmission computed tomography imaging system. J Nucl Med 33:1881-1887, 1992
11. Hasegawa BH, Lang TF, Brown EL, et al. Object specific attenuation correction of SPECT with correlated dual-energy X-ray CT. IEEE Trans Nucl Sci NS-40:1242-1252, 1993
12. Blankespoor SC, Wu X, Kalki K, et al: Attenuation correction of SPECT using X-ray CT on an emission-transmission CT system: Myocardial perfusion assessment. IEEE Trans Nucl Sci 43:2263-2274, 1996
13. Tang HR, Da Silva AJ, Matthay KK, et al: Neuroblastoma imaging using a combined CT scanner-scintillation camera and 131I-MIBG. J Nucl Med 42:237-47, 2001
14. Beyer T, Kinahan PE, Townsend DW, et al: The use of X-ray CT for attenuation correction of PET data. Nuclear Science Symposium and Medical Imaging Conference, 1994, 1994 IEEE Conference Record 4:1573-1577 vol. 4, 1994
15. Beyer T, Townsend DW, Brun T, et al: A combined PET/CT scanner for clinical oncology. J Nucl Med 41:1369-1379, 2000

16. Kinahan PE, Townsend DW, Beyer T, et al: Attenuation correction for a combined 3D PET/CT scanner. Med Phys 25:2046-2053, 1998
17. Charron M, Beyer T, Bohnen NN, et al: Image analysis in patients with cancer studied with a combined PET and CT scanner. Clin Nucl Med 25:905-10, 2000
18. Kluetz PG, Meltzer CC, Villemagne VL, et al: Combined PET/CT imaging in oncology. Impact on patient management. Clin Positron Imaging 3:223-230, 2000
19. Meltzer CC, Luketich JD, Friedman D, et al: Whole-body FDG positron emission tomographic imaging for staging esophageal cancer comparison with computed tomography. Clin Nucl Med 25:882-887, 2000
20. Patton JA, Delbeke D, Sandler MP: Image fusion using an integrated, dual-head coincidence camera with X-ray tube-based attenuation maps. J Nucl Med 41:1364-1368, 2000
21. Bocher M, Balan A, Krausz Y, et al: Gamma camera-mounted anatomical X-ray tomography: Technology, system characteristics and first images. Eur J Nucl Med 27:619-627, 2000
22. Surti S, Kuhn A, Werner ME, et al: Performance of philips gemini TF PET/CT scanner with special consideration for its time-of-flight imaging capabilities. J Nucl Med 48:471-480, 2007
23. Kalender WA, Seissler W, Klotz E, et al: Spiral volumetric CT with single-breath-hold technique, continuous transport, and continuous scanner rotation. Radiology 176:181-183, 1990
24. Schardt P, Deuringer J, Freudenberger J, et al: New x-ray tube performance in computed tomography by introducing the rotating envelope tube technology. Med Phys 31:2699-2706, 2004
25. Takagi K, Fukazawa T: Cerium-activated $Gd_2SiO_5$ single crystal scintillator. App Phys Lett 42:43-45, 1983
26. Melcher CL, Schweitzer JS: Cerium-doped lutetium oxyorthosilicate: A fast, efficient new scintillator. IEEE Trans Nucl Sci 39:502-505, 1992
27. Townsend DW, Isoardi RA, Bendriem B. Volume imaging tomographs, in Bendriem B, Townsend DW (eds): The Theory and Practice of 3D PET. Dordrecht, Kluwer Academic Publishers, 1998, pp 111-132
28. Kemp BJ, Kim C, Williams JJ, et al, National Electrical Manufacturers Association (NEMA): NEMA NU 2-2001 performance measurements of an LYSO-based PET/CT system in 2D and 3D acquisition modes. J Nucl Med 47:1960-1967, 2006
29. Strobel K, Rudy M, Treyer V, et al: Objective and subjective comparison of standard 2-D and fully 3-D reconstructed data on a PET/CT system. Nucl Med Commun 28:555-559, 2007
30. Jakoby BW, Bercier Y, Watson CC, et al: Physical performance and clinical workflow of a new LSO HI-REZ PET/CT scanner. Nuclear Science Symposium Conference Record, 2006 IEEE 5:3130-3134, 2006
31. Townsend DW, Jakoby B, Long MJ, et al. Performance and clinical workflow of a new combined PET/CT scanner. J Nucl Med 48:437P, 2007
32. Budinger TF: Time-of-flight positron emission tomography: Status relative to conventional PET. J Nucl Med 24:73-78, 1983
33. Muehllehner G, Karp JS: Positron emission tomography. Phys Med Biol 51:R117-37, 2006
34. Kinahan PE, Rodgers JG: Analytic 3D image reconstruction using all detected events. IEEE Trans Nucl Sci 36:964-968, 1989
35. Defrise M, Kinahan PE, Townsend DW, Michel C, Sibomana M, Newport DF: Exact and approximate rebinning algorithms for 3-D PET data. IEEE Trans Med Imaging 16:145-158, 1997
36. Hudson H, Larkin R: Accelerated image reconstruction using ordered subsets of projection data. IEEE Trans Med Imaging 13:601-609, 1994
37. Comtat C, Kinahan PE, Defrise M, et al: Fast reconstruction of 3D PET data with accurate statistical modeling. IEEE Trans Nucl Sci 45:1083-1089, 1998
38. Comtat C, Bataille F, Michel C, et al: OSEM-3D reconstruction strategies for the ECAT HRRT. Nuclear Science Symposium Conference Record, 2004 IEEE 6:3492-3496, 2004
39. Liu X, Comtat C, Michel C, et al: Comparison of 3-D reconstruction with 3D-OSEM and with FORE+OSEM for PET. IEEE Trans Med Imaging 20:804-814, 2001
40. Panin VY, Kehren F, Michel C, et al: Fully 3-D PET reconstruction with system matrix derived from point source measurements. IEEE Trans Med Imaging 25:907-921, 2006
41. Popescu LM, Matej S, Lewitt RM. Iterative image reconstruction using geometrically ordered subsets with list-mode data. Nuclear Science Symposium Conference Record, 2004 IEEE 6:3536–3540, 2004
42. Daube-Witherspoon ME, Matej S, Karp JS, et al: Application of the row action maximum likelihood algorithm with spherical basis functions to clinical PET imaging. IEEE Trans Nucl Sci 48:24-30, 2001
43. Kinahan PE, Hasegawa BH, Beyer T: X-ray-based attenuation correction for positron emission tomography/computed tomography scanners. Semin Nucl Med 33:166-179, 2003
44. Watson CC, Townsend DW, Bendriem B. PET/CT systems, in Wernick M, Aarsvold J (eds): Emission Tomography. London, Elsevier Science, 2004, pp 195-212
45. Burger C, Goerres G, Schoenes S, et al: PET attenuation coefficients from CT images: Experimental evaluation of the transformation of CT into PET 511-keV attenuation coefficients. Eur J Nucl Med Mol Imaging 29:922-927, 2002
46. Watson CC, Rappoport V, Faul D, et al: A method for calibrating the CT-based attenuation correction of PET in human tissue. IEEE Trans Nucl Sci 53:102-107, 2006
47. Carney JP, Townsend DW, Rappoport V, et al: Method for transforming CT images for attenuation correction in PET/CT imaging. Med Phys 33:976-983, 2006
48. Cohade C, Wahl RL: Applications of positron emission tomography/computed tomography image fusion in clinical positron emission tomography-clinical use, interpretation methods, diagnostic improvements. Semin Nucl Med 33:228-237, 2003
49. Bockisch A, Beyer T, Antoch G, et al: Positron emission tomography/computed tomography–imaging protocols, artifacts, and pitfalls. Mol Imaging Biol 6:188-199, 2004
50. Nakamoto Y, Chin BB, Cohade C, et al: PET/CT: Artifacts caused by bowel motion. Nucl Med Commun 25:221-225, 2004
51. Cohade C, Osman M, Marshall L, et al: Metallic object artifacts on PET-CT: Clinical and phantom studies. J Nucl Med 43:308P, 2002
52. Goerres GW, Ziegler SI, Burger C, et al: Artifacts at PET and PET/CT caused by metallic hip prosthetic material. Radiology 226:577-584, 2003
53. Kamel EM, Burger C, Buck A, et al: Impact of metallic dental implants on CT-based attenuation correction in a combined PET/CT scanner. Eur Radiol 13:724-728, 2003
54. Yau YY, Coel M, Chan WS, et al: Application of IV contrast in PET-CT: Does it really produce attenuation correction error. J Nucl Med 44: 272P, 2003
55. Antoch G, Freudenberg LS, Beyer T, et al: To enhance or not to enhance? 18F-FDG and CT contrast agents in dual-modality 18F-FDG PET/CT. J Nucl Med 45:56S-65S, 2004 (suppl 1)
56. Carney JP, Beyer T, Brasse D, et al: Clinical PET/CT scanning using oral CT contrast agents. J Nucl Med 45:57P, 2002
57. Cohade C, Osman M, Nakamoto Y, et al: Initial experience with oral contrast in PET/CT: Phantom and clinical studies. J Nucl Med 44:412-416, 2003
58. Schafers KP, Raupach R, Beyer T: Combined 18F-FDG-PET/CT imaging of the head and neck. An approach to metal artifact correction. Nuklearmedizin 45:219-222, 2006
59. Lemmens C, Nuyts J, Faul D, et al: Suppression of metal streak artifacts in CT using a MAP reconstruction procedure. IEEE MIC Conference Record 6:3431-3437, 2006
60. Mirzaei S, Guerchaft M, Bonnier C, et al: Use of segmented CT transmission map to avoid metal artifacts in PET images by a PET-CT device. BMC Nucl Med 5:3, 2005
61. Sarikaya I, Yeung HW, Erdi Y, et al: Respiratory artefact causing malpositioning of liver dome lesion in right lower lung. Clin Nucl Med 28:943-944, 2003
62. Romer W, Chung M, Chan A, et al: Single-detector helical CT in

PET-CT: Assessment of image quality. AJR Am J Roentgenol 182:1571-1577, 2004
63. Osman MM, Cohade C, Nakamoto Y, et al: Clinically significant inaccurate localization of lesions with PET/CT: Frequency in 300 patients. J Nucl Med 44:240-243, 2003
64. Carney JP, Townsend DW: CT-based attenuation correction for PET/CT scanners, in von Schulthess GK (ed): Molecular Anatomic Imaging: PET-CT and SPECT-CT Integrated Modality Imaging. Lippincott, Williams and Wilkins, 2006, pp 54-62
65. Antoch G, Freudenberg LS, Egelhof T, et al: Focal tracer uptake: A potential artifact in contrast-enhanced dual-modality PET/CT scans. J Nucl Med 43:1339-1342, 2002
66. Berthelsen AK, Holm S, Loft A, et al: PET/CT with intravenous contrast can be used for PET attenuation correction in cancer patients. Eur J Nucl Med Mol Imaging 32:1167-1175, 2005
67. Mawlawi O, Erasmus JJ, Munden RF, et al: Quantifying the effect of IV contrast media on integrated PET/CT: Clinical evaluation. AJR Am J Roentgenol 186:308-319, 2006
68. Brechtel K, Klein M, Vogel M, et al: Optimized contrast-enhanced CT protocols for diagnostic whole-body 18F-FDG PET/CT: Technical aspects of single-phase versus multiphase CT imaging. J Nucl Med 47: 470-476, 2006
69. Gollub MJ, Hong R, Sarasohn DM, et al: Limitations of CT during PET/CT. J Nucl Med 48:1583-1591, 2007
70. Otsuka H, Graham MM, Kubo A, et al: The effect of oral contrast on large bowel activity in FDG-PET/CT. Ann Nucl Med 19:101-108, 2005
71. Antoch G, Kuehl H, Kanja J, et al: Dual-modality PET/CT scanning with negative oral contrast agent to avoid artifacts: Introduction and evaluation. Radiology 230:879-885, 2004
72. Kaneta T, Takanami K, Wakayama Y, et al: High-density materials do not always induce artifacts on PET/CT: What is responsible for the difference? Nucl Med Commun 28:495-499, 2007
73. Beyer T, Antoch G, Blodgett T, et al: Dual-modality PET/CT imaging: The effect of respiratory motion on combined image quality in clinical oncology. Eur J Nucl Med Mol Imaging 30:588-596, 2003
74. Osman MM, Cohade C, Nakamoto Y, et al: Respiratory motion artifacts on PET emission images obtained using CT attenuation correction on PET-CT. Eur J Nucl Med Mol Imaging 30:603-606, 2003
75. Papathanassiou D, Becker S, Amir R, et al: Respiratory motion artefact in the liver dome on FDG PET/CT: Comparison of attenuation correction with CT and a caesium external source. Eur J Nucl Med Mol Imaging 32:1422-1428, 2005
76. Bacharach SL: PET/CT attenuation correction: Breathing lessons. J Nucl Med 48:677-679, 2007
77. Beyer T, Rosenbaum S, Veit P, et al: Respiration artifacts in whole-body (18)F-FDG PET/CT studies with combined PET/CT tomographs employing spiral CT technology with 1 to 16 detector rows. Eur J Nucl Med Mol Imaging 32:1429-1439, 2005
78. Pan T, Mawlawi O, Nehmeh SA, et al: Attenuation correction of PET images with respiration-averaged CT images in PET/CT. J Nucl Med 46:1481-1487, 2005
79. Chi PC, Mawlawi O, Nehmeh SA, et al: Design of respiration averaged CT for attenuation correction of the PET data from PET/CT. Med Phys 34:2039-2047, 2007
80. Alessio AM, Kohlmyer S, Branch K, et al: Cine CT for attenuation correction in cardiac PET/CT. J Nucl Med 48:794-801, 2007
81. Pan T, Lee TY, Rietzel E, et al: 4D-CT imaging of a volume influenced by respiratory motion on multi-slice CT. Med Phys 31:333-340, 2004
82. Meirelles GS, Erdi YE, Nehmeh SA, et al: Deep-inspiration breath-hold PET/CT: Clinical findings with a new technique for detection and characterization of thoracic lesions. J Nucl Med 48:712-719, 2007
83. Nehmeh SA, Erdi YE, Meirelles GS, et al: Deep-inspiration breath-hold PET/CT of the thorax. J Nucl Med 48:22-26, 2007
84. Dawood M, Buther F, Lang N, et al: Respiratory gating in positron emission tomography: A quantitative comparison of different gating schemes. Med Phys 34:3067, 2007
85. Martinez-Moller A, Zikic D, Botnar RM, et al: Dual cardiac-respiratory gated PET: Implementation and results from a feasibility study. Eur J Nucl Med Mol Imaging 34:1447-1454, 2007
86. Nagel CC, Bosmans G, Dekker AL, et al: Phased attenuation correction in respiration correlated computed tomography/positron emitted tomography. Med Phys 33:1840-1847, 2006
87. Allen-Auerbach M, Yeom K, Park J, et al: Standard PET/CT of the chest during shallow breathing is inadequate for comprehensive staging of lung cancer. J Nucl Med 47:298-301, 2006
88. Beyer T, Bockisch A, Kuhl H, et al: Whole-body 18F-FDG PET/CT in the presence of truncation artifacts. J Nucl Med 47:91-99, 2006
89. Carney JP, Townsend DW, Kinahan PE, et al. CT-based attenuation correction: The effects of imaging with the arms in the field of view [abstract]. J Nucl Med Soc Nucl Med 42S:56P-57P, 2001
90. Mawlawi O, Pan T, Cody DD, et al: Evaluation of a new CT truncation correction algorithm for accurate quantification of PET/CT images [abstract]. J Nucl Med 45S:413P, 2004
91. Zaidi H: Is radionuclide transmission scanning obsolete for dual-modality PET/CT systems? Eur J Nucl Med Mol Imaging 34:815-818, 2007
92. Nakamoto Y, Osman M, Cohade C, et al: PET/CT: Comparison of quantitative tracer uptake between germanium and CT transmission attenuation-corrected images. J Nucl Med 43:1137-1143, 2002
93. van Dalen JA, Visser EP, Vogel WV, et al: Impact of ge-68/Ga-68-based versus CT-based attenuation correction on PET. Med Phys 34: 889-897, 2007
94. Brix G, Beyer T. PET/CT: Dose-escalated image fusion? Nuklearmedizin 44:S51-S57, 2005 (suppl 1)
95. ICRP 87: Managing Patient Dose in Computed Tomography. Oxford, New York, Published for the International Commission on Radiological Protection by Pergamon, 2000
96. Brix G, Lechel U, Glatting G, et al: Radiation exposure of patients undergoing whole-body dual-modality 18F-FDG PET/CT examinations. J Nucl Med 46:608-613, 2005
97. Kalender WA, Wolf H, Suess C, et al: Dose reduction in CT by on-line tube current control: Principles and validation on phantoms and cadavers. Eur Radiol 9:323-328, 1999
98. Kachelriess M, Watzke O, Kalender WA: Generalized multi-dimensional adaptive filtering for conventional and spiral single-slice, multi-slice, and cone-beam CT. Med Phys 28:475-490, 2001
99. ICRP 53: Radiation Dose to Patients from Radiopharmaceuticals: Addendum 2 to ICRP Publication 53. Oxford, New York, Published for the International Commission on Radiological Protection by Pergamon, 1999
100. Deloar HM, Fujiwara T, Shidahara M, et al: Estimation of absorbed dose for 2-[F-18]fluoro-2-deoxy-D-glucose using whole-body positron emission tomography and magnetic resonance imaging. Eur J Nucl Med 25:565-574, 1998
101. Hays MT, Watson EE, Thomas SR, et al: MIRD dose estimate report no. 19: Radiation absorbed dose estimates from (18)F-FDG. J Nucl Med 43:210-214, 2002
102. Czernin J, Auerbach MA. Clinical PET/CT imaging: Promises and misconceptions. Nuklearmedizin 44:S18-S23, 2005 (suppl 1)
103. Czernin J, Allen-Auerbach M, Schelbert HR: Improvements in cancer staging with PET/CT: Literature-based evidence as of september 2006. J Nucl Med 48:78S-88S, 2007 (suppl 1)
104. Israel O, Kuten A: Early detection of cancer recurrence: 18F-FDG PET/CT can make a difference in diagnosis and patient care. J Nucl Med 48:28S-35S, 2007 (suppl 1)
105. Chen YK, Su CT, Ding HJ, et al: Clinical usefulness of fused PET/CT compared with PET alone or CT alone in nasopharyngeal carcinoma patients. Anticancer Res 26:1471-1477, 2006
106. Palmedo H, Bucerius J, Joe A, et al: Integrated PET/CT in differentiated thyroid cancer: Diagnostic accuracy and impact on patient management. J Nucl Med 47:616-624, 2006
107. Osman MM, Cohade C, Leal J, et al: Direct comparison of FDG-PET and PET-CT imaging in staging and re-staging patients with lung cancer. J Nucl Med 43:151P, 2002
108. Lardinois D, Weder W, Hany TF, et al: Staging of non-small-cell lung

cancer with integrated positron-emission tomography and computed tomography. N Engl J Med 348:2500-2507, 2003
109. Cerfolio RJ, Bryant AS, Ojha B: Restaging patients with N2 (stage IIIa) non-small cell lung cancer after neoadjuvant chemoradiotherapy: A prospective study. J Thorac Cardiovasc Surg 131:1229-1235, 2006
110. Fueger BJ, Weber WA, Quon A, et al: Performance of 2-deoxy-2-[F-18]fluoro-D-glucose positron emission tomography and integrated PET/CT in restaged breast cancer patients. Mol Imaging Biol 7:369-376, 2005
111. Tatsumi M, Cohade C, Mourtzikos KA, et al: Initial experience with FDG-PET/CT in the evaluation of breast cancer. Eur J Nucl Med Mol Imaging 33:254-262, 2006
112. Bar-Shalom R, Guralnik L, Tsalic M, et al: The additional value of PET/CT over PET in FDG imaging of oesophageal cancer. Eur J Nucl Med Mol Imaging 32:918-924, 2005
113. Guo H, Zhu H, Xi Y, et al: Diagnostic and prognostic value of 18F-FDG PET/CT for patients with suspected recurrence from squamous cell carcinoma of the esophagus. J Nucl Med 48:1251-1258, 2007
114. Cohade C, Osman M, Leal J, Wahl RL: Direct comparison of (18)F-FDG PET and PET/CT in patients with colorectal carcinoma. J Nucl Med 44:1797-1803, 2003
115. Kim JH, Czernin J, Allen-Auerbach MS, et al: Comparison between 18F-FDG PET, in-line PET/CT, and software fusion for restaging of recurrent colorectal cancer. J Nucl Med 46:587-595, 2005
116. Reinhardt MJ, Joe AY, Jaeger U, et al: Diagnostic performance of whole body dual modality 18F-FDG PET/CT imaging for N- and M-staging of malignant melanoma: Experience with 250 consecutive patients. J Clin Oncol 24:1178-1187, 2006
117. Freudenberg LS, Antoch G, Schutt P, et al: FDG-PET/CT in re-staging of patients with lymphoma. Eur J Nucl Med Mol Imaging 31:325-329, 2004
118. Yi CA, Lee KS, Kim BT, et al: Tissue characterization of solitary pulmonary nodule: Comparative study between helical dynamic CT and integrated PET/CT. J Nucl Med 47:443-450, 2006
119. Kim SK, Allen-Auerbach M, Goldin J, et al: Accuracy of PET/CT in characterization of solitary pulmonary lesions. J Nucl Med 48:214-220, 2007
120. Alavi A, Mavi A, Basu S, Fischman A: Is PET-CT the only option? Eur J Nucl Med Mol Imaging 34:819-821, 2007
121. Coleman RE, Delbeke D, Guiberteau MJ, et al: Concurrent PET/CT with an integrated imaging system: Intersociety dialogue from the joint working group of the American college of radiology, the society of nuclear medicine, and the society of computed body tomography and magnetic resonance. J Nucl Med 46:1225-1239, 2005